Link to Journal website - http://www.nrcresearchpress.com/journal/cgj

Title

In situ measurement of root-reinforcement using the corkscrew extraction method

Authors

G. J. Meijer[1,2,3*]

A. G. Bengough[1,3]

J. A. Knappett[1]

K. W. Loades[3]

B. C. Nicoll[2]

1: University of Dundee, School of Science and Engineering, Dundee DD1 4HN, UK

2: Forest Research, Northern Research Station, Roslin, Midlothian EH25 9SY, UK

3: James Hutton Institute, Invergowrie, Dundee DD2 5DA, UK

*: Corresponding author, g.j.z.meijer@dundee.ac.uk, telephone +44(0)1382 386083

Abstract

Mechanical root-reinforcement is an important parameter to evaluate for stability analysis of rooted slopes. The contribution of roots is however difficult to quantify in situ without time-consuming methods or heavy equipment. Here we report field testing using the newly developed 'corkscrew' method at two different sites with plant with conifers and blackcurrant. In both sites we found positive correlations between root quantity and root-reinforcement in surface layers where many roots were found. Below 125 mm depth, no correlations could be found, probably due to variability in soil stress and gravel content. Roots were shown not only to increase the soil peak strength but also to add ductility to the soil, i.e. adding strength over much larger displacement ranges. Measured reinforcements, although similar to other experimental studies, was lower than predicted using existing models. This may be attributed to the distinct difference in shear displacement required to mobilise the strength of soil and roots. By the time roots are mobilising their strength, the soil strength component has reduced from peak to a much lower residual strength. The 'corkscrew' method proved a promising tool to quantify root-reinforcement in field conditions due to its ease of use and short test duration.

Key words: Root-reinforcement, cork screw, vegetation, *in situ* testing, slope stability

1 Introduction

It is well known that roots can positively increase soil strength through reinforcing soil as inclusions inducing a mechanical effect. Part of the soil shear load is taken up by the roots and transferred to other parts of the soil through root stretching and root–soil interface friction (Coppin and Richards 1990; Gray and Sotir 1996; Norris et al. 2008; Stokes et al. 2009). Their contribution is however difficult to quantify due to limited understanding of interaction processes between roots and soil and because of the large spatial and temporal variation in root properties, root architecture and soil properties.

The direct shear test is commonly used to directly measure the strength of rooted soil in situ. Various designs have been proposed (Wu et al. 1979; Endo 1980; Hengchaovanich and Nilaweera 1996; Ekanayake et al. 1997; Wu and Watson 1998; Cammeraat et al. 2005; Docker and Hubble 2008; Fan and Su 2008; Comino et al. 2010). Generally, the shear plane in these tests lay between 0 and 0.5 m depth, with the notable exception of Hengchaovanich and Nilaweera (1996) who measured up to 1.5 m depth. These tests are however highly destructive, time-consuming and require heavy equipment, making them less suitable to be applied on difficult terrain. This makes them unsuitable for characterising large areas and assessing variability of rooted soil shear characteristics.

Another commonly adopted strategy to quantify root reinforcement is to measure root quantity, diameter and tensile strength and convert this data into an additional soil cohesion term ('root cohesion' c_r) using a model. Roots can be quantified for example by counting roots on trench walls (e.g. Abdi et al. 2010; Abernethy and Rutherfurd 2001; Mao et al. 2012; Moos et al. 2016) or core sampling (e.g. Ammer and Wagner 2005; Danjon et al. 2008; Genet et al. 2008; Wang et al. 2006). The Wu/Waldron model (WWM) is the most well-known model and possibly the most used (Waldron 1977; Wu et al. 1979), linking root tensile strength (σ_t) and root cross-sectional area ratio (A_r) to an increase in soil cohesion:

$$c_r = k' \sigma_t \frac{A_r}{A} \tag{1}$$

where A is the area of the shear plane and $k' = 1.2$, a factor based on the average angle at which strained roots cross the shear plane and an average angle of soil internal friction. The fraction of the shear area occupied by root cross section (A/A_r) is commonly referred to as the root area ratio RAR. By summing the effects of individual roots, the total increase in strength can be obtained, i.e.:

$$c_r = k' \sum_{i=1}^{n} \sigma_{t,i} RAR_i \tag{2}$$

Root strength and stiffness are often found to be diameter-dependent and fitted with power laws in the form:

$$\sigma \text{ or } E = \alpha d_r^{\beta} \tag{3}$$

where α and β are fitting coefficients.

A major shortcoming of the WMW approach is the inherent assumption that all roots break simultaneously, and the model is often shown to overestimate reinforcement (e.g. Operstein and Frydman 2000; Preti 2013; Wu and Watson 1998). To take sequential breakage into account, fibre bundle models (FBM) have been proposed by Pollen and Simon (2005). In these models, the total load is distributed among

the remaining intact roots in a user-defined way. Once the tensile force exceeds the strength in a single root, the load it carries is distributed over remaining intact roots. Incrementally increasing the load until all roots have failed yields the maximum force the bundle can sustain. An important modelling choice is how to distribute the load over roots with different properties. Often this is done based on the root diameter. Then, the force in root i (F_i) can be described by:

$$F_i = F \frac{d_{r,i}^a}{\sum_{j=1}^{n} d_{r,j}^a} \tag{4}$$

where $d_{r,i}$ the diameter of root i, n the total number of intact roots, F the total applied force and a a dimensionless distribution factor. Common choices of a are $a = 0$, meaning that the load is equally distributed over all roots, regardless of the diameter, and $a = 2$, resulting in equal stresses in all roots. When $a > 2 + \beta_\sigma$ (β_σ in the tensile strength–diameter relation of Equation 3), the thickest roots will break first, while when $a < 2 + \beta_\sigma$ thinner roots will break first. When $a = 2 + \beta_\sigma$, all roots will fail at the same time, equalling the WWM. As in experimental testing it is commonly observed that smaller roots break first, often equal load sharing ($a = 0$) is adopted (e.g. Comino and Marengo 2010; Thomas and Pollen-Bankhead 2010), although these studies seem to overlook that any value $0 < a < 2 + \beta_\sigma$ might accomplish similar dynamics. Others distribute the load based on root elasticity (e.g. Schwarz et al. 2010). In terms of Equation 4, this means $a = 2 + \beta_E$, with β_E the power constant in the diameter–elasticity relation (Equation 3).

When a reduction factor due to progressive root failure (k'') is incorporated into the WWM, the root cohesion can be expressed as:

$$c_r = k' k'' \sum_{i=1}^{n} \sigma_{t,i} RAR_i \tag{5}$$

A wide range of values for k'' is reported, for example $k'' = 0.55$–1.00 (Mao et al. 2012), 0.45–0.82 (Pollen and Simon 2005) and 0.35-0.56 (Adhikari et al. 2013).

The accuracy of quantifying root-reinforcement by combining root counts with interpretative models depends strongly on the accuracy of sampling and the reliability of the adopted model. Root sampling is very time-consuming, making it difficult to survey large sections of slopes. Conducting a large number of tests might however be important to find weak zones on the slope where landslides are more likely to occur.

To address the need for a new, quicker and easy to transport soil measurement method capable of accurately including the additional reinforcement introduced by roots, Meijer et al. (2016) proposed various new approaches. One of these is the corkscrew method. In summary, the 'corkscrew' is rotated into the soil and then vertically extracted while measuring force and displacement. Rotational installation ensures that the soil and roots are disturbed minimally, as only the soil in the path of the screw tip will be disturbed. This contrasts strongly with the use of a field shear vane, for which was shown that in fibrous peats a lot of disturbance occurs during vane installation as fibres are pushed aside or break under the vane blades (Landva 1980). During cork screw extraction, shear forces will mobilise around the interface of the soil cylinder trapped within the helix of the screw (Figure 1b). Since the dimensions of the screw are known, this force can be used to calculate the shear resistance along the interface. This

method detected both the presence of thick root analogues and the effect of abundant fibres laboratory experiments (Meijer et al. 2016). In unrooted ('fallow') field soil, at a depth > 250 mm similar peak strengths were measured when compared to a standard field vane (Meijer et al. 2015).

However, the 'corkscrew' method has not yet been validated under field conditions including real vegetation (e.g. with variability in root and soil properties). This paper will apply the method at two field sites with contrasting species (one field with shrubs and one with trees) and results are compared to the WWM and fibre bundle models.

2 Methods

2.1 Field sites

Measurements were performed on two sites. The first site was Bullionfield (Figure 6), near the James Hutton Institute, Invergowrie, UK (56°27'31.3"N, 3°04'15.1"W). This field was planted in April 2012 with 1 year old potted Blackcurrant (*Ribes nigrum*) shrubs. Shrubs were planted in lines with 0.4 m between each plant. The distance between each line was approximately 2.8 m. Between each line, a 1.7 m wide strip of grass was present (Figures 5-6). No other vegetation was present near the shrubs. The soil was classified as slightly clayey sand (British Standards Institution 2004). Atterberg limits were $w_P = 18\%$ and $w_L = 25\%$. Testing was performed over three successive days in December 2015.

The second site was Hallyburton Hill forest (Figure 8), a Forestry Commission owned woodland in the Sidlaw Hills, near Dundee, UK (56°31'10.3"N, 3°11'29.9"W), planted in 1962 with mature Sitka spruce (*Picea sitchensis*). The soil was classified as sandy silt (Atterberg limits: $w_P = 35\%$, $w_L = 56\%$). Testing was performed on two plots over the course of four days in December 2014. On the first day, corkscrew tests were performed in a relatively open forest patch (plot 1). On days 2–4, testing was performed in a denser region of forest (Plot 2). The plots were spaced approximately 10–15 m apart (Figures 7-8). Particle size distributions for both sites can be found in Figure 9.

On both sites soil dry bulk density and water content were measured adjacent to the testing location. Soil physical properties were measured using 100 ml steel cores. Soil suctions were measured *in situ* using field tensiometers (model SWT4R, Delta-T, Cambridge, UK). Suctions were not measured and assumed to be <2 kPa in Bullionfield because of abundant rainfall in the weeks before testing, resulting in high water tables (visually present at 150–250 mm depth). Soil horizon depths were manually determined based on visual observation in soil pits and compared with the Soil Information for Scottish Soils database (James Hutton Institute 2016). Results for both sites are compared in Figure 10.

2.2 Root mechanical characteristics

A large number of roots were sampled to determine their biomechanical strength and stiffness properties, both in tension and 3-point bending. Sampled roots were bagged and stored in a fridge at 4°C for a maximum of 4 days prior to testing to eliminate potential decomposition effects, similar to Loades et al. (2013).

Depending on the root diameter, a universal testing machine (Instron 5966) was fitted with a 50 N, 500 N or 2 kN load cell, using the smallest load cell possible without overloading. Sixty blackcurrant roots with diameter d_r ranging between 0.45 and 9.17 mm and a length of 40, 60, 80 or 100 mm were tested in uniaxial tension. Root length over diameter ratio was at least 10 to minimise the influence of clamping. All roots were tested at a rate of 5% strain per minute, in line with loading rates reported in literature (1–10 mm min^{-1}, e.g. Genet et al. (2008); Loades et al. (2010)). Root ends were clamped using pneumatic clamps with a pressure of 100 kPa ($0 \leq d_r \leq 2$ mm), 200 kPa ($2 \leq d_r \leq 5$ mm) or 300 kPa ($d_r > 5$ mm). For roots with diameters exceeding approximately 3 mm it was necessary to peel off bark at root ends prior to testing to ensure good grip. Removing bark was unlikely to have influenced results with observations during testing showing that all load carrying was concentrated in the central stele region of roots. Seventy-six Sitka spruce roots ($0.39 \leq d_r \leq 10.2$ mm), all with a length of 100 mm, were also tested for tensile strength and stiffness using the same test conditions. The methods and results for biomechanical testing on Sitka spruce roots were described earlier in Meijer et al. (2017a).

Forty-eight blackcurrant roots ($0.64 \leq d_r \leq 11.75$ mm) were tested in three-point bending, using a loading rate of 5 mm min^{-1}, a maximum displacement of 50 mm and a support span of at least 10 L/d_r. Although a value of $L/d_r \geq 20$ is recommended for testing of wood and timber (Rowe et al. 2006), sampled root lengths and/or changing root properties over the length of the root, e.g. excessive tapering, made this inappropriate. Sixty-two Sitka spruce roots ($0.52 \leq d_r \leq 26.5$ mm) were tested in bending using the same test conditions. In all but two of the thickest Sitka spruce roots ($d_r > 24$ mm) the support span/root diameter ratio was smaller than 10 (7.5–8.0).

For all roots, the peak strength, Young's modulus (stiffness over the elastic region) and secant stiffness at 90% of the peak strength (E_{90}) were determined. The latter parameter provides some insight into the non-linear stress–strain behaviour of the roots. Root properties versus diameter relationships were fitted using conventional power law fits, see Equation 3.

2.3 Corkscrew device and setup

For both sites, a similar screw, supplied as a garden corkscrew weeder (De Wit, Kornhorn, The Netherlands), was used. The height of the screws was h_{cs} = 120–125 mm, the diameter d_{cs} = 40 mm, the diameter of the helix 6 mm and the helix pitch approximately 28 mm (Figure 2), similar to Meijer et al. (2015, 2016). The ratio between the volume of the corkscrew and the volume of the extracted soil cylinder is 8.9%, which is below the allowance for field shear vanes (maximum ratio 12%, British Standards Institution 1990). Therefore the influence of corkscrew installation on soil disturbance can be considered to be within acceptable limits.

The axial stiffness of the corkscrew helix (k_{cs}) was determined in compression over a range of 0–600 N using a universal testing machine (model 5966, Instron, High Wycombe, UK) and found be highly linear over this force interval, resulting in k_{cs} = 54.3 Nmm^{-1}. The tensile stiffness was assumed to be equal to the compression stiffness.

A laboratory setup for initial trialling of the technique was previously described by Meijer et al. (2016) and a field setup by Meijer et al. (2015), see Figure 3. The screw was installed by hand-rotation and

then attached using a steel cable to a winch mounted on a tripod. The load in this cable was measured using a 5 kN load cell (model RLT05000kg, RDP Group, Wolverhampton, UK) and the displacement of the screw by using a draw wire sensor (model WDS-1500-P60-CR-P, Micro-Epsilon, Birkenhead, UK). Both load and displacement were measured at 100 Hz using a data logger. The pull-out rate was on average 120 mm min^{-1}, in line with the displacement rate of slow landslides (Davies et al. 2010) and previous studies (Meijer et al. 2015). Pull-out displacement was applied by a hand winch with a ratchet. In combination with a stopwatch, The ratcheting sounds were used to control the displacement rate.

2.4 Corkscrew data interpretation – root-reinforcement

Corkscrew extraction yields force–displacement traces, similar to the result of a direct shear test (Figure 1a). Thus the full shear stress–strain behaviour of the root-reinforcement soil is recorded. Root-reinforcement can be found by subtracting the fallow soil behaviour from the rooted soil behaviour.

Because the corkscrew is slightly flexible the recorded draw wire displacements will be greater than the vertical displacement of the soil. Therefore the 'average' soil displacement was estimated as the displacement u halfway along the corkscrew, defined as:

$$u = u^* - \frac{1}{2}\frac{F(u^*)}{k_{cs}} \tag{6}$$

where u^* is the measured displacement, $F(u^*)$ the measured extraction force at displacement level u^* and k_{cs} the screw axial stiffness.

The peak root-reinforced shear strength measured with the corkscrew ($\tau_{cs,peak}$) was calculated as:

$$\tau_{cs,peak} = \frac{F(u_{peak})}{\pi d_{cs} h_{cs}} \tag{7}$$

where $F(u_{peak})$ is the maximum extraction force occurring at displacement u_{peak}, the displacement at peak shear strength, and d_{cs} and h_{cs} the corkscrew diameter and height respectively.

The residual strength measured with the corkscrew was calculated as:

$$\tau_{cs,res} = \min\left(\frac{F(u)}{\pi d_{cs} h_{cs}}\right),\ u_{peak} \leq u \leq h_{cs} \tag{8}$$

At the shallowest tested depth level (0–120/125 mm), no residual strength could be accurately determined because of the formation of a wedge-like failure (Figure 4a). This affected tests performed at 120–240/125–250 as well, since because soil near the surface is removed the shear area will decrease during the test (Figure 4b). Therefore at this depth the residual strength was defined as:

$$\tau_{cs,res} = \min\left(\frac{F(u)}{\pi d_{cs}(h_{cs} - u)}\right),\ u_{peak} \leq u \leq h_{cs} \tag{9}$$

The contribution of root-reinforcement to direct shearing is not only characterised by the increase in peak shear strength also by a certain shear displacement range over which this reinforcement is active. To capture this 'ductility' component of the reinforcement in a single parameter (as identified in Meijer et al. (2016)), a normalised energy dissipation parameter (W_n) is introduced. This dimensionless parameter is defined as the total work required to move the corkscrew from $u = u_1$ to $u = u_2$, normalised over the

product of peak force (F_{peak}) and displacement, i.e.:

$$W_n = \frac{1}{F_{peak}(u_1 - u_0)} \int_{u_0}^{u_1} F(u)du \tag{10}$$

W_n therefore serves as an indicator for the 'average' root-reinforced soil strength over a certain displacement range with respect to the peak strength ($0 \leq W_n \leq 1$). In this study, $u_0 = 0$ mm and $u_1 = 100$ mm were chosen. The latter limit was chosen as test results show that typically roots failed at displacements $u < 100$ mm (see Figure 16).

2.5 Corkscrew data interpretation – behaviour of individual roots

Apart from providing shear stress–strain data for the (root-reinforced) soil, the corkscrew force–displacement data might also potentially be used to identify individual roots and their characteristics. Some roots might be visible as distinct 'root peaks' in the force–displacement trace (see Figure 1a); a root will provide reinforcement until it breaks, visible as a sudden decrease in cork screw pull-out resistance. Such behaviour was observed in previous corkscrew laboratory tests using root analogues (Meijer et al. 2015) and preliminary field trials (Meijer et al. 2016). These force drops bear a strong resemblance to those observed during penetrometer testing in rooted soil using a penetrometer with an adapted tip shape to increase the penetrometer sensitivity to roots ('blade penetrometer' Meijer et al. 2015, 2017b,a). These 'root peaks' have two characteristics: a) the magnitude of the sudden decrease in resistance ('force drop', root peak force F_u) and b) the root displacement required to reach this point (root peak displacement u_u), see Figure 1a. The main advantage of identifying these individual 'root peaks' is that they provide information about the kind of roots present in the soil. Thus, for example, one might establish whether reinforcement is primarily caused to coarse roots or due to fine roots, without the need for excavation.

Meijer et al. (2017b) developed two interpretative models, linking F_u and u_u to root strength, root stiffness and lateral and axial soil resistance parameters. The two models assume root failure in either pure bending or pure tension (see Meijer et al. (2017b) for full model descriptions and derivations).

The 'bending model' is based on solving the Euler-Bernoulli differential equation for beam bending:

$$E_b I \frac{\partial^4 w}{\partial x^4} = -d_r p_u \tag{11}$$

where E_b is the root bending stiffness, I the second moment of inertia, d_r the root diameter, p_u the lateral soil resistance per unit root length×root diameter and w the lateral root displacement. The lateral soil resistance was modelled as rigid perfectly plastic, i.e. the full soil resistance is mobilised after infinitesimally small root displacements. This is justified as root displacements are typically much larger than those required for the soil to mobilise full resistance. The root is considered to have failed once the bending stress exceeds the root strength anywhere in the root.

The 'cable model' assumed roots had no bending stiffness and failing in pure tension, equal to a cable. Assuming parabolic deformation, the displaced shape and corresponding stresses were found using the fact that the increase in root length due to axial loading should equal the increase in arc length of the deformed root shape.

For both the bending and cable model, solutions for roots loaded by a point load and roots loaded by shearing soil along part of the root length were derived. These are summarised in Table 1. For thick roots, considering the corkscrew loading as a point load might be important due to the limited diameter of the corkscrew with respect to the length of the displacing root (Figure 1c), while for thinner roots a loading assuming shear loading might be more appropriate (Figure 1d). These two loading cases can be seen as upper and lower bounds. As a final and fifth model, measured values for F_u were directly compared to the maximum tensile force the root can sustain in uniaxial tension ('tensile strength model').

When reasonable values for root properties (strength and stiffness) and soil parameters (soil resistance to root deformation) can be measured or assumed, these models can be used to predict diameters of roots crossing the shear plane between the cork screw and surrounding soil based on F_u or u_u. Thus information on whether the measured root-reinforcement is mostly generated by thicker roots (which are more likely to generate clearly identifiable 'root peaks') or by fine roots.

In this paper, values for the root–soil interface friction τ_i were estimated based on the measured standard vane shear strength and multiplied by 0.5 after Mickovski et al. (2009) to take into account that the root–soil interface friction is lower than soil–soil interface friction. Values for the ultimate soil–root perpendicular resistance p_u were based on standard penetrometer testing performed at both sites, using a ∅12 mm 30° tip connected to a ∅10 mm shaft. The measured resistance was multiplied by $\alpha_2 = 0.623$ to account for shape differences between a cone-shaped penetrometer and a cylindrically-shaped root. α_2 was determined by comparing experimentally measured standard penetrometer results to the model for soil resistance against laterally displacing piles derived by Reese and Van Impe (2011) for piles in dry sand, see Meijer et al. (2017b). Where the interpretative models require a root stiffness value, the secant stiffness at 90% strength (E_{90}) was used rather than Young's modulus over the linear-elastic region (E) to capture the non-linear stress–strain behaviour more accurately (Meijer et al. 2017a).

In this work, where the magnitude of the force drop (F_u) could easily be identified in corkscrew traces, they were compared to the diameter of thick root ends identified during excavation following corkscrew testing. The largest drop was linked to the largest diameter root found, the second largest drop to the second largest root etc.

2.6 Corkscrew data collection

In Bullionfield, corkscrew tests were gathered over the course of two days. Tests were performed at 0–120, 120–240 mm and 240–360 mm depth sequentially with each test at increasing depth within the hole left open by the previous test at shallower depth. If the target installation depth could not be reached, e.g. because of large stones, the actual installation depth was recorded and the results calculated for the smaller shear plane area.

At Hallyburton Hill, on day 1 results were gathered on plot 1. On days 2 to 4, tests were done on plot 2. Corkscrew test data from day 3 were lost due to a data logger error. The range of distances between test points and the nearest tree varied: on day 1 it ranged between 1.2 and 2.0 m, on day 2 between 0.9 and 1.5 m and on day 4 between 0.3 and 1.1 m. On the first two days, at every one of the 5 measurement locations tests were performed at 0–125, 125–250, 250–375 and 375–500 mm depth. On

day 4, a further 11 locations were tested but measurements were only taken at 0–125 and 125–250 depth. It was decided to increase the number of tests at shallow depths because work done on the first two days indicated that root quantities were low at depths below 250 mm at this site. In Figure 7 the locations of test plots, corkscrew tests and nearby trees are given.

All corkscrew tests were spaced at least $10d_{cs}$ apart, so that there was no interaction between tests. The potential zone of influence resulting from testing was calculated using the model of Chattopadhyay and Pise (1986) for soil deformation around foundation piles tested in tension. Assuming a soil angle of internal friction of $\phi = 30°$, soil–'pile' interface friction angle $\delta = \phi$ and 'pile' depth of 500 mm, the radius of the uplifted soil wedge at the surface was estimated to be $4.47d_{cs}$.

At both sites, a number of standard shear vane measurements were collected using a 50 mm high 34 mm diameter cruciform blade (Edeco Pilcon, Simmons Edeco inc., Calgary, Canada). Both peak and residual strengths were recorded. At Bullionfield, 16 successful tests were performed over a depth range of 0–300 mm. At Hallyburton Hill a total of 43 measurements were taken a depth range of 0–500 mm.

2.7 Sampling and processing of extracted corkscrew samples

After each corkscrew test, the extracted corkscrew soil cores were wrapped in cling film and subsequently stored in a freezer (-30°C). The volume of the frozen cores were measured using a ruler (1 mm divisions) and weighed using a balance (accurate to 0.01 g). Each sample was analysed for broken root ends protruding from the sides of the core. To make these more visible, the sides of the frozen cores were sprayed with hot water to remove soil, exposing the roots. Root end depths were recorded and their diameters measured using a microscope fitted with an eyepiece graticule (10 mm long with 0.1 mm ticks). The largest magnification, 4.0, 3.0, 2.0, 1.0 or 0.7×, for which the whole root diameter could be captured in the graticule was used. Thus an accuracy of roughly $d_r/100$ was achieved. Only roots with a diameter exceeding 0.5 mm were measured as it proved difficult to establish whether thinner roots were broken.

After quantifying all root ends, samples were carefully washed, collecting all root material and larger soil particles on a 2 mm sieve. All roots were subsequently scanned and analysed using WinRhizo (version 2003b) using uniform diameter classes with a width of 0.1 mm. Soil particles retained on the 2 mm sieve were oven-dried and dry sieved using 2, 4, 8 and 20 mm sieves and their mass measured. To establish particle size mass fractions, the dry weights of the sampled cores were required. This required the soil water content, which could not be directly measured due to the root sampling procedure. Therefore the linear soil water content–depth fit from Figure 10 was used to estimate the water content in each sample.

Since water expands slightly during freezing, the measured densities using the frozen core dimensions and mass underestimated the real densities *in situ*. Therefore a correction factor was established by averaging the ratio between frozen densities and density estimates using the linear density–depth fits established using steel core samples (Figure 10). For every depth and site a different correction factor was determined. In this way realistic densities were acquired for each extracted corkscrew core while maintaining information on the natural variation in corkscrew sample densities. These densities were used to estimate the total vertical soil stress in the field at the centre of each corkscrew test.

Holes in the soil left open after corkscrew testing were filled with polyurethane expanding foam to

trap broken root ends left in the external wall of the extracted cylinder. At Bullionfield, foam was applied one week after testing to allow soil to drain following heavy rain. However, no foam could be applied below approximately 250 mm because of the water table level. These problems did not arise at Hallyburton Hill because of a lower water table. After the foam had set, foam casts and the surrounding soil were dug up. Excess soil was washed away, and subsequently root end depths and diameters were established in a similar fashion as for extracted corkscrew samples (Figure 11).

The root end count results from both extracted corkscrew samples and foam cores were summed to get a full set of all root ends passing though the shear surface. Since only root ends with diameters exceeding 0.5 mm were counted, the results from root scanning were used to fill the gap between $0 \leq d_r < 0.5$ mm. The WinRhizo root volumes were transformed to root area ratios by assuming random orientations of the roots, so $RAR = 0.5RV$ (Bengough et al. 1992), where RAR is the root area ratio [m^2 m^{-2}] and RV the root volume fraction [m^3 m^{-3}].

2.8 Root-reinforcement predictions and data analysis

The experimental results for the measured root-reinforcement were compared to predictions made based on the Wu/Waldron model (WWM) and various fibre bundle models (FBM). Separate FBM predictions were made with differing load sharing parameters (a = 0, 1 or 2). For every corkscrew measurement, simulations were run for every FBM using the measured root area ratios and root properties to find k'', the reduction factor for mechanical reinforcement due to progressive root failure.

Statistical analyses were performed using R statistical software (R Core Team 2013). Statistical significance of p-values is reported as three levels: $p > 0.05$: n.s. (not significant); $p \leq 0.05$: *; $p \leq 0.01$: **; $p \leq 0.001$: ***.

3 Results

3.1 Root mechanical properties

The results for root strength and elasticity for both Sitka spruce and blackcurrant roots, both in tension and bending, can be found in Figure 12. Both the strength and stiffness of blackcurrant roots appeared independent of root diameter ($\beta \approx 0$) while for Sitka spruce roots mostly positive relations were found. The only statistically significant ($p \leq 0.05$) values for the power coefficient β were found for all Sitka spruce bending properties and E_{90} measured on Sitka spruce in tension. All other β-values were non-significant, reflecting the variation in a natural material such as root tissue.

3.2 Root distributions

Root quantities decreased rapidly with depth at both sites (Figure 13). At both sites, the majority of the root volume consisted of fine roots (d_r = 0–2 mm) although at Hallyburton roots with diameters exceeding 2 mm were more abundant than in Bullionfield. At Hallyburton Hill, more thick roots ($d_r > 5$

mm) and less fine roots were found on day 4, reflecting the smaller distance to the nearest tree compared to measurements on earlier days. The total amount of thick roots was highly variable between samples.

Root area ratios determined using WinRhizo (assuming uniform distributions of the roots with random orientations) generally yielded higher results compared to measuring root ends sticking out of the corkscrew and foam cores, especially for fine (0.5–2 mm) roots (Figure 14). There may be a number of explanations for this: 1) roots growing vertically, resulting in fewer intersections with the vertical shear plane; 2) root ends that were not found during counting of roots in corkscrew and foam cores; or 3) inaccuracies in WinRhizo.

3.3 Cork screw shear strengths

On average, the maximum (root-reinforced) shear strengths measured with the corkscrew were slightly lower than standard vane readings (Figure 15), but both followed similar depth trends. Standard vane peak strength readings showed considerable scatter. Residual shear strengths were significantly lower than peak strengths for both measurement methods, indicating that both soils possessed some measure of sensitivity, commonly defined as the ratio between peak and residual strength. Measured sensitivities were $S_t = 2$–6 in the surface layer (0–120/125 mm depth) and $S_t = 5$–13 at higher depths. Note that in this paper S_t is defined as the ratio between root-reinforced peak and residual soil shear strength.

A number of example corkscrew force–displacement traces for each site and measurement depth level are shown in Figure 16. In both sites, tests conducted near the surface showed a marked difference in the force–displacement behaviour between tests with large and small values for RAR. Individual root failures could be distinguished where the force suddenly drops rapidly over the course of 10–50 ms. Large roots failures occurred at displacements ($u \approx 50$–100 mm), much higher than those required to reach peak resistance in tests with low RAR ($u \approx 5$–10 mm). This shows that roots mobilise their strength at large shear strains compared to fallow soil.

A strong positive correlation between measured corkscrew peak strength and the sum of root tensile strength was found in the surface layers (0–120/125 mm depth) at both sites (Figure 17). In deeper layers (> 125 mm) however, no significant or negative correlations were found.

At Hallyburton Hill positive correlations were found between total vertical soil stress and peak strength at depths > 125 mm, some statistically significant. However, although results appear to indicate that variations in peak strength at depths > 125 mm were mainly caused by variations in soil stress, the low stress values were unlikely to have caused such a great variation in soil shear strength when realistic values for the soil angle of internal friction are assumed. At Bullionfield these correlations were weaker.

When the peak strength was compared to the quantity of gravel ($d \geq 2$ mm) measured in extracted corkscrew cores from Hallyburton Hill, positive but non-significant correlations were found, with an especially steep gradient at 375–500 mm depth. At Bullionfield, peak strength and gravel appeared to be uncorrelated, except at 240–360 mm depth where a weak negative correlation was found.

Part of the negative relationship between peak strength and roots at greater depths may be explained by looking at the relation between soil stresses and root volumes (Figure 18). Only fine roots ($d_r \leq 2$ mm) were used in this analysis to obtain a more reliable estimate of distribution of roots in the soil due

to large individual thick roots likely to have a very large influence on the results. At depths >120–125 mm at both sites, either no correlation or a non-significant negative correlations were found between fine roots and soil stress. At 375–500 mm depth at Hallyburton Hill, a significant negative correlation was found between fine root volume and soil stress. This suggests that in these deeper layers, roots preferentially grow where the soil stress levels are locally reduced. This is in line with a reduction in root growth found in soils with increased mechanical impedance (Bengough and Mullins 1990).

The encountered variation in soil parameters at depths greater than 120 mm made it difficult to relate the increase in soil strength to the effect of root inclusions, due to the variation in reinforced soil strength not only being related to variations in roots but also to variations in density and gravel content of the soil. These factors cannot be treated as independent, since root growth does depend on soil impedance and it is likely that gravel content relates to both soil strength (different material behaviour) and soil density (different soil structure). Only where the soil strength was low and roots were plentiful, i.e. near the surface, a strong and significant positive correlations between roots and soil strength were found.

3.4 Normalised energy dissipation

An example graph for the normalised energy dissipation parameter W_n for the heaviest and least rooted soil at 120–240 mm depth at Bullionfield can be found in Figure 19, showing distinct differences in the shape of the extraction curve and therefore in W_n.

In both sites, within the surface layers (0–125 mm) strong positive correlations were present between root strength and W_n, and positive trends were also found at 125–250 mm depth. Below 250 mm, root quantities were small and did not significantly affect W_n (Figure 20). The positive correlation between W_n and root strength shows that the soil behaves with increased ductility when roots are present, in addition to increasing the peak strength. Total vertical soil stress did not significantly affect W_n. However, at Bullionfield the presence of gravel was found to affect W_n between 0 and 240 mm depth; more gravel resulted in significantly smaller values for W_n. An hypothesis for the latter effect could be dislodging of stones by the corkscrew. Stones intersecting the shear plane could increase the peak strength but might get dislodged after sufficient corkscrew displacement. This would lead to an increase in S_t and therefore a reduction in W_n.

3.5 Relative contributions of root diameter classes

To establish the relative effect of fine ($0 \leq d_r < 2$), medium ($2 \leq d_r < 5$) and thick roots ($d_r \geq 5$ mm) on the measured variation in peak shear strength and W_n in the surface layer (0–125 mm), a Type I analysis of variance (ANOVA) was performed. This showed at Bullionfield the variation in the measured peak shear strength was best explained by fine roots (d_r = 0–2 mm). However, although larger roots barely influence the peak strength, they have considerable influence on W_n. At Hallyburton Hill, the large roots (>5 mm) were the main contributors to both root strength and W_n (Table 2).

3.6 Comparison between remeasured and predicted root-reinforcement

WWM and FBM model predictions for the increase in shear strength due to roots yielded widely ranging predictions (Figure 22). Predictions were only made for the surface layer (0–125 mm) because only in these a clear relationship between roots and an increase in the soil peak shear strength were found (Figure 17). All models significantly overestimated the reinforcement measured in the experiments. The WWM is the simplest model, only requiring RAR and σ_t as input parameters, but yielded the most inaccurate predictions. Fibre bundle models, requiring additional information on root diameter distributions and a load sharing parameter, provided more accurate predictions, but still overestimated the measured reinforcement significantly. The FBM load distribution parameter a has a large effect on the predicted reinforcement.

3.7 Behaviour of individual roots

During corkscrew testing 46 clear sudden drops in extraction force (F_u) were identified. The interpretative models described earlier were used to predict the root diameter of the corresponding roots, based on estimated values of p_u and τ_i (based on penetrometer data) and root diameter–root strength and root diameter–root stiffness relationships (based on tensile and 3-point bending tests described earlier).

Clear positive trends were observed between the predicted diameter based on the magnitude of the sudden force drop in penetrometer resistance (F_u) and the measured diameters of excavated roots (Figure 21). For Sitka spruce roots in Hallyburton Hill, the results suggests a model assuming tensile failure works best, although some of the thicker roots ($d_r > 6$ mm) might have failed in bending. Results for Blackcurrant roots in Bullionfield display more scatter but appears to follow similar trends. The variation in the experimental data however makes it difficult to establish which model is most accurate.

4 Discussion

4.1 Root mechanical properties

It is widely reported that decreasing tensile strength is associated with increasing root diameter, e.g. see Mao et al. (2012). Values for *Picea abies* reported by Vergani et al. (2014) showed a range between $-0.17 \leq \alpha_\sigma \leq 0.13$, depending on the sampling site (original fits reported in terms of force), more in line with values found in this study, indicating negative power law relationships between root diameter and strength or stiffness are not always suitable. Data on tensile stiffness is very scarce, and no data on bending properties was found in the literature apart from a study by Stokes et al. (1996) using 5 mm diameter core samples taken from first order lateral tree roots.

Root biomechanical properties are not just a function of species and diameter. Root strength was shown to vary as a function of root water content and root age (Burylo et al. 2011; Genet et al. 2008), decomposition (e.g. O'Loughlin and Ziemer 1982), soil conditions such as the water content (Loades et al. 2010), root type (Loades et al. 2013) or environmental condition (e.g. trees on slopes; Stokes et al. 2002; Abdi et al. 2010). More work is required to yield more accurate predictions for root biomechanical

properties.

4.2 Comparison of corkscrew to shear vane strength

The peak shear strength measured using the corkscrew was generally lower than measured with the shear vane. This can be explained by number of reasons: 1) Shear vanes are developed for measuring the undrained shear strength of cohesive soils. Therefore, the underlying assumption is that the shear resistance is independent from the soil stress. When used in granular soils however, the average normal stress on the shear plane might increase as part of the lateral pressure applied by a vane blade will be transferred as normal load to the shear plane, therefore increasing the shear resistance. Therefore, the shear vane is likely to overestimate the soil shear strength. This effect will not be present in cork screw testing as the direction of loading and the shear plane are parallel to each other, similar to direct shear tests conditions. Caution is therefore required when comparing vane to corkscrew results. 2) Near the surface, the corkscrew showed a cone-like failure mechanism during testing in the surface layer (0–120/125 mm), likely to have resulted in an underestimation of the actual shear strength. Therefore corkscrew testing can be considered to yield conservative results near the surface. Cone-like failure offers a reason why corkscrew tests gave slightly lower peak strength results compared to the standard vane device in surface layers. 3) The vane device is smaller than the corkscrew, and therefore more sensitive to spatial variability in the soil, especially where pockets of gravel are present. The presence of a single stone near the shear plane can have a large effect on the measured vane shear strength. This does explain the large variability in measured vane strengths compared to strengths measured using the corkscrew. 4) At increased depths the corkscrew pull-out resistance is higher, causing more strain in the corkscrew helix. This will cause a slight gradient of soil strain over the test depth and might therefore cause a slight reduction in the measured strength, as the peak strength does not mobilise simultaneously along the shear plane. The vane device is much less sensitive to this effect since it is stiffer.

The large difference between peak and residual root-reinforced strength can be attributed to three effects: 1) roots failing during shearing, 2) light cementation of the soil, or 3) soil structure. While the roots will have some effect, even tests with small values of RAR show considerable sensitivity, indicating that cementation and/or soil is present within the soil. To check whether measured vane residual strengths are realistic, results were compared to values estimated using a simple model (Fredlund and Rahardjo 1993) to estimate the shear strength of unsaturated soil on a vertical plane (Figure 23):

$$\tau = c + (\sigma_v + s)\tan\phi \tag{12}$$

where σ_v is the total vertical soil stress, s the suction pressure, c the soil cohesion (assumed at 5 kPa) and ϕ the soil angle of internal friction (assumed as 30°). At Bullionfield, suctions were assumed to be negligible because of the high rainfall prior to testing and the high water table. At Hallyburton Hill, a constant $s \approx 6$ kPa is assumed, based on field measurements (Figure 10), but only below 80 mm depth. At depths < 80 mm soil measured densities were very low resulting in large voids and capillaries which were considered to be too wide to hold significant suctions. Although Equation 12 predicts the shear strength for horizontal planes while the vane device largely measures shear strength on vertical ones,

Figure 23 suggests that the vane residual strengths measured were accurate and not just an artefact of the measurement procedure. Measured values for the residual cork screw strengths were generally higher than residual values measured using the vane device. Significant differences occurring below 250 mm depth in plot 1 of Hallyburton Hill. In this plot, the soil horizon containing lots of parent material ('BC') was located relatively shallow. It is hypothesised that large stones might have got stuck between the corkscrew helix, therefore effecting the behaviour well into residual strain ranges. In vane tests, stones might have simply been pushed aside, therefore not affecting the shear behaviour at large deformations.

4.3 Comparison of measured reinforcement to model predictions

The experimentally measured root-reinforcement to soil shearing was much lower than conventional model predictions. Several potential reasons were identified:

1) The soil was shown to possess sensitivity, i.e. the ratio between peak and residual strength is pronounced. Since roots mobilise resistance at much higher displacements than soil (Ekanayake et al. 1997; Mickovski et al. 2009), it is likely that the full reinforcement only mobilises when the soil strength is declining towards residual strength. This will result in a lower apparent reinforcing effect when peak strengths are compared, see Figure 24. This effect will be more pronounced in more sensitive soils. Natural field soils may age-harden in time through reorientation or cementation (Utomo and Dexter 1981; Dexter 1988) and therefore sensitivity may increase over time. In these soils, the root-reinforced peak strength will be lower than the sum of fallow soil peak strength and root cohesion. Therefore, we suggest that this effect should be studied in more detail in future work.

2) All existing models assume that all roots with similar diameters fail simultaneously, even in FBMs. However, this negates the effect of different root orientations. Variation in root orientation means that roots with similar diameters will mobilise resistance progressively, potentially resulting in lower predicted reinforcements, especially when roots within a particular size class drive root reinforcement (Table 2). Furthermore, when the soil is rooted with predominantly fine roots, they would predict a high reinforcement peak present over only a short displacement interval since cable model predicts fine roots only need small displacements to fully mobilise their strength. However, in reality, instead of one big peak the reinforcement is present over much larger displacements and the soil behaves in a very ductile way (e.g. Comino et al. 2010; Operstein and Frydman 2000). This suggests that these models do not capture the right root reinforcement mobilisation mechanism, especially for finer roots.

3) Example corkscrew traces (Figure 16) show that large roots have a large effect on the reinforcement results (Vergani et al. 2014). All models assume that these large roots break in tension. However, in reality they might fail first in bending resulting in potentially higher model results. Furthermore, it might have been the case that these thicker roots slipped out of the corkscrew during the test rather than breaking, providing another potential reason that measured reinforcement was lower.

Experimental root-reinforcement results in the surface layers (0–120/125 mm) were compared against other studies. Values for k' were similar but at the lower end of those found in the literature (Figure 25). Interestingly k' values acquired in controlled conditions (laboratory) are lower than those found in the field testing. Laboratory values were all derived from saturated (Pollen and Simon 2005; Operstein

and Frydman 2000) or near-saturated (Loades et al. 2010, saturated and subsequently drained at 5 kPa suction) conditions. All field data was derived from soil at natural water contents, apart from Docker and Hubble (2008) who tested in saturated conditions.

4.4 Behaviour of individual roots

The scatter observed in the comparison between measured root diameters and those predicted based on force drops (F_u) observed in corkscrew force–displacement traces made it difficult to establish which interpretative model is the most accurate. This scatter could stem from numerous sources, such as the scatter observed in root diameter–root strength and root diameter–root stiffness relationships (Figure 12) or the methodology followed to estimate soil resistance parameters p_u and τ_i. Furthermore, all models assume roots as cylinders with homogeneous, linear elastic material behaviour, even though root stress-strain behaviour exhibits plasticity (e.g. Loades et al. 2013) and the root cross-section consists of various tissues with different functions (e.g. Gregory 2006). To deal with the natural variation in these properties, more experimental data is required. The preliminary results shown here do show the potential of extracting additional useful information about roots, apart from root-reinforcement values, from measured shear force–displacement data.

5 Conclusions

- The corkscrew method measured root-reinforcement in surface layers, in which there was an abundance of roots. Peak strength values were greater where more roots were present. Deeper in soil mechanical reinforcement was hidden by spatial variations in soil properties, as shown by variation in soil stress and gravel content.

- Negative correlations between soil strength and root presence suggest roots grow where the soil is locally weak. This means that root cohesion is not merely a constant factor in slope stability modelling but reinforces the soil where it needs it most. The corkscrew test, because it is much faster than direct shear testing in the field, offers a relatively rapid way of obtaining shear strength data of root–reinforced soil at varying depths.

- The presence of roots significantly altered the shape of the soil stress-strain curves measured by the corkscrew. Roots added reinforcement over much larger displacement ranges than typically considered when studying non-rooted soils. Roots were shown to enhance the amount of energy required to shear the soil beyond strains to reach peak resistance in non-rooted (or sparsely rooted) soil significantly. This additional ductility might be important when large deformation problems such as landslide propagation are studied.

- Various existing reinforcement prediction models yield very different results depending on the model and model parameters chosen. However, all overestimated the measured reinforcement. This is probably caused by stress–strain behaviour of the soil, as large differences between peak and residual shear strength were identified. Roots were observed to mobilise their strength at much

larger shear displacements than the soil. This means the peak strength of the root-reinforced soil is not simply equal to the sum of the non-rooted soil peak strength and the calculated root cohesion, in contrast to common practice. We suggest that in future studies both root and soil stress–strain behaviour is investigated in more detail.

- Additional information on the diameter of some of the roots crossing the shear plane could be extracted from the magnitude of sudden drops in measured corkscrew resistance associated with failure of individual roots, given estimations for root strength, root stiffness and the lateral and axial soil resistance to relative soil–root displacement are available. However, the results were inconclusive about which interpretative model is most reliable.

- The corkscrew proved a useful tool for measuring root-reinforcement in field conditions. It is a quick test requiring simple and light equipment, simple to install in rooted soils without causing too much disturbance due to its self-drilling helical shape, and the results are easy to interpret. This allows for testing at various locations on sites with difficult access. Future work should focus on extending the database of field data, preferably at a site with less sensitive soil (i.e. with a smaller difference between peak and residual strength). Other suggestions include studying the influence of wedge formation near the surface, as well as the precise mechanism of root mobilisation.

Acknowledgements

The authors want to thank David Boldrin (University of Dundee/James Hutton Institute) and Colin McEvoy (Forest Reseach) for their help during field experiments. G. J. Meijer acknowledges a studentship provided by Forest Research, funded by ClimateXChange, the Scottish Government's Centre for Expertise on Climate Change. The James Hutton Institute receives funding from the Scottish Government.

References

Abdi, E., Majnounian, B., Genet, M., and Rahimi, H. (2010). Quantifying the effects of root reinforcement of Persian ironwood (*Parrotia persica*) on slope stability; a case study: Hillslope of Hyrcanian forests, northern Iran. *Ecological Engineering*, 36(10):1409–1416.

Abernethy, B. and Rutherfurd, I. D. (2001). The distribution and strength of riparian tree roots in relation to riverbank reinforcement. *Hydrological Processes*, 15(1):63–79.

Adhikari, A. R., Gautam, M. R., Yu, Z., Imada, S., and Acharya, K. (2013). Estimation of root cohesion for desert shrub species in the Lower Colorado riparian ecosystem and its potential for streambank stabilization. *Ecological Engineering*, 51:33–44.

Ammer, C. and Wagner, S. (2005). An approach for modelling the mean fine-root biomass of Norway spruce stands. *Trees – Structure and Function*, 19(2):145–153.

Bengough, A. G., Mackenzie, C. J., and Diggle, A. J. (1992). Relations between root length densities and root intersections with horizontal and vertical planes using root growth modelling in 3-dimensions. *Plant and Soil*, 145(2):245–252.

Bengough, A. G. and Mullins, C. E. (1990). Mechanical impedance to root growth: a review of experimental techniques and root growth responses. *Journal of Soil Science*, 41(3):341–358.

British Standards Institution (1990). BS 1377-9:1990: Methods of test for soils for civil engineering purposes – part 9: In-situ tests.

British Standards Institution (2004). BS EN ISO 14688-2:2004+A1:2013: Geotechnical investigation and testing – identification and classification of soil.

Burylo, M., Hudek, C., and Rey, F. (2011). Soil reinforcement by the roots of six dominant species on eroded mountainous marly slopes (Southern Alps, France). *Catena*, 84(1–2):70–78.

Cammeraat, E., van Beek, R., and Kooijman, A. (2005). Vegetation succession and its consequences for slope stability in SE Spain. *Plant and Soil*, 278(1–2):135–147.

Chattopadhyay, B. C. and Pise, P. J. (1986). Uplift capacity of piles in sand. *Journal of Geotechnical Engineering (ASCE)*, 12(9):888–904.

Comino, E. and Marengo, P. (2010). Root tensile strength of three shrub species: *Rosa canina*, *Cotoneaster dammeri* and *Juniperus horizontalis*. *Catena*, 82(3):227–235.

Comino, E., Marengo, P., and Rolli, V. (2010). Root reinforcement effect of different grass species: A comparison between experimental and models results. *Soil & Tillage Research*, 110(1):60–68.

Coppin, N. and Richards, I. (1990). *Use of vegetation in civil engineering, CIRIA book 10*. Butterworths, Kent.

613 Danjon, F., Barker, D. H., Drexhage, M., and Stokes, A. (2008). Using three-dimensional plant root
614 architecture in models of shallow-slope stability. *Annals of Botany*, 101(8):1281–1293.

615 Davies, M. C. R., Bowman, E. T., and White, D. J. (2010). Physical modelling of natural hazards. In
616 Springman, S., Laue, J., and Seward, L., editors, *Physical modelling in geotechnics, ICPMG 2010*,
617 pages 3–22, London. Taylor and Francis.

618 Dexter, A. R. (1988). Advances in characterization of soil structure. *Soil & Tillage Research*, 11(3–
619 4):199–238.

620 Docker, B. B. and Hubble, T. C. T. (2008). Quantifying root-reinforcement of river bank soils by four
621 Australian tree species. *Geomorphology*, 100(3–4):401–418.

622 Ekanayake, J. C., Marden, M., Watson, A. J., and Rowan, D. (1997). Tree roots and slope stability: a
623 comparison between *Pinus radiata* and kanuka. *New Zealand Journal of Forestry Science*, 27(2):216–
624 233.

625 Endo, T. (1980). Effect of tree roots upon the shear-strength of soil. *Japan Agricultural Research*
626 *Quarterly*, 14(2):112–115.

627 Fan, C.-C. and Su, C.-F. (2008). Role of roots in the shear strength of root-reinforced soils with high
628 moisture content. *Ecological Engineering*, 33(2):157–166.

629 Fredlund, D. G. and Rahardjo, H. (1993). *Soil mechanics for unsaturated soils.* John Wiley & Sons Inc.,
630 New York.

631 Genet, M., Kokutse, N., Stokes, A., Fourcaud, T., Cai, X., Ji, J., and Mickovski, S. (2008). Root
632 reinforcement in plantations of *Cryptomeria japonica* D. Don: effect of tree age and stand structure
633 on slope stability. *Forest Ecology and Management*, 256(8):1517–1526.

634 Gray, D. H. and Sotir, R. B. (1996). *Biotechnical and soil bioengineering slope stabilization, a practical*
635 *guide for erosion control.* John Wiley & Sons Inc, New York.

636 Gregory, P. J. (2006). *Plant roots: growth, activity and interaction with soils.* Blackwell Publishing,
637 Oxford.

638 Hengchaovanich, D. and Nilaweera, N. S. (1996). An assessment of strength properties of vetiver grass
639 roots in relation to slope stabilization. In *Proceedings of the International Conference on Vetiver,*
640 *Chain Kai, Thailand*, pages 153–158, Bangkok, Thailand. Office of the Royal Development Projects
641 Board.

642 James Hutton Institute (2016). Soil information for Scottish soils (SIFFS).

643 Landva, A. O. (1980). Vane testing in peat. *Canadian Geotechnical Journal*, 17(1):1–19.

644 Loades, K. W., Bengough, A. G., Bransby, M. F., and Hallett, P. D. (2010). Planting density influence
645 on fibrous root reinforcement of soils. *Ecological Engineering*, 36(3):276–284.

Loades, K. W., Bengough, A. G., Bransby, M. F., and Hallett, P. D. (2013). Biomechanics of nodal, seminal and lateral roots of barley: effects of diameter, waterlogging and mechanical impedance. *Plant and Soil*, 370(1):407–418.

Mao, Z., Saint-Andre, L., Genet, M., Mine, F.-X., Jourdan, C., Rey, H., Courbaud, B., and Stokes, A. (2012). Engineering ecological protection against landslides in diverse mountain forests: Choosing cohesion models. *Ecological Engineering*, 45:55–69.

Meijer, G. J., Bengough, A. G., Knappett, J. A., Loades, K. W., and Nicoll, B. C. (2015). Comparison of new in situ root-reinforcement measuring devices to existing techniques. In Winter, M., Smith, D., Eldred, P., and Toll, D., editors, *Proceedings of the 16th European Conference on Soil Mecanics and Geotechnical Engineering (XVI ECSMGE): Geotechnical Engineering for Infrastructure and Development*, pages 1621–1626, London. Institution of Civil Engineers.

Meijer, G. J., Bengough, A. G., Knappett, J. A., Loades, K. W., and Nicoll, B. C. (2016). New in-site techniques for measuring the properties of root-reinforced soil – laboratory evaluation. *Géotechnique*, 66(1):27–40.

Meijer, G. J., Bengough, A. G., Knappett, J. A., Loades, K. W., and Nicoll, B. C. (2017a). In situ root identification through blade penetrometer testing – part 2: field testing. *Géotechnique*. Ahead of print.

Meijer, G. J., Bengough, A. G., Knappett, J. A., Loades, K. W., Nicoll, B. C., Mukov, I., and Zhang, M. (2017b). In situ root identification through blade penetrometer testing – part 1: interpretative models and laboratory testing. *Géotechnique*. Ahead of print.

Mickovski, S. B., Hallett, P. D., Bransby, M. F., Davies, M. C. R., Sonnenberg, R., and Bengough, A. G. (2009). Mechanical reinforcement of soil by willow roots: Impacts of root properties and root failure mechanism. *Soil Science Society of America Journal*, 73(4):1276–1285.

Moos, C., Bebi, P., Graf, F., Mattli, J., Rickli, C., and Schwarz, M. (2016). How does forest structure affect root reinforcement and susceptibility to shallow landslides? *Earth Surface Processes and Landforms*, 41(7):951–960.

Norris, J. E., Stokes, A., Mickovski, S. B., Cammeraat, E., Van Beek, R., Nicoll, B. C., and Achim, A. (2008). *Slope stability and erosion control: Ecotechnical solutions*. Springer, Dordrecht, The Netherlands.

O'Loughlin, C. and Ziemer, R. R. (1982). The importance of root strength and deterioration rates upon edaphic stability in steepland forests. In *I.U.F.R.O. Workshop P.1.07-00 Ecology of Subalpine Ecosystems as a Key to Management*, pages 70–78, Courvallis, Oregon. Oregon State University.

Operstein, V. and Frydman, S. (2000). The influence of vegetation on soil strength. *Ground Improvement*, 4:81–89.

Pollen, N. and Simon, A. (2005). Estimating the mechanical effects of riparian vegetation on stream bank stability using a fiber bundle model. *Water Resources Research*, 41(7):W07025.

Preti, F. (2013). Forest protection and protection forest: Tree root degradation over hydrological shallow landslides triggering. *Ecological Engineering*, 61, Part C:633–645.

R Core Team (2013). *R: A Language and Environment for Statistical Computing*. R Foundation for Statistical Computing, Vienna, Austria.

Reese, L. C. and Van Impe, W. F. (2011). *Single piles and pile groups under lateral loading, 2nd edition*. CRC, Leiden, The Netherlands.

Rowe, N. P., Isnard, S., Gallebmüller, F., and Speck, T. (2006). Diversity of mechanical architectures in climbing plants: an ecological perspective. In Herrel, A., Speck, T., and Rowe, N., editors, *Ecology and biomechanics: a mechanical approach to the ecology of animals and plants*, pages 35–60. CRC, Boca Raton, FL, US.

Schwarz, M., Lehmann, P., and Or, D. (2010). Quantifying lateral root reinforcement in steep slopes – from a bundle of roots to tree stands. *Earth Surface Processes and Landforms*, 35(3):354–367.

Stokes, A., Atger, C., Bengough, A. G., Fourcaud, T., and Sidle, R. C. (2009). Desirable plant root traits for protecting natural and engineered slopes against landslides. *Plant and Soil*, 324(1–2):1–30.

Stokes, A., Ball, J., Fitter, A. H., Brain, P., and Coutts, M. P. (1996). An experimental investigation of the resistance of model root systems to uprooting. *Annals of Botany*, 78(4):415–421.

Stokes, A., Fourcaud, T., Hruska, J., Çermák, J., Nadyezdhina, N., Nadyezhdin, V., and Praus, L. (2002). An evaluation of different methods to investigate root system architecture of urban trees in situ: I. ground-penetrating radar. *Journal of Arboriculture*, 28(1):2–10.

Thomas, R. E. and Pollen-Bankhead, N. (2010). Modeling root-reinforcement with a fiber-bundle model and Monte Carlo simulation. *Ecological Engineering*, 36(1):47–61.

Utomo, W. H. and Dexter, A. R. (1981). Age hardening of agricultural top soils. *Journal of Soil Science*, 32(3):335–350.

Vergani, C., Schwarz, M., Cohen, D., Thormann, J. J., and Bischetti, G. B. (2014). Effects of root tensile force and diameter distribution variability on root reinforcement in the Swiss and Italian Alps. *Canadian Journal of Forest Research*, 44(11):1426–1440.

Waldron, L. J. (1977). Shear resistance of root-permeated homogeneous and stratified soil. *Soil Science Society of America Journal*, 41(5):843–849.

Wang, Z., Wang, D., Wang, X., Gu, J., and Mei, L. (2006). Fine root architecture, morphology, and biomass of different branch orders of two Chinese temperate tree species. *Plant and Soil*, 288(1–2):155–171.

Wu, T. H., McKinnell III, W. P., and Swanston, D. N. (1979). Strength of tree roots and landslides on Prince of Wales Island, Alaska. *Canadian Geotechnical Journal*, 16(1):19–33.

Wu, T. H. and Watson, A. (1998). In situ shear tests of soil blocks with roots. *Canadian Geotechnical Journal*, 35(4):579–590.

Tables

Table 1: Analytical solutions for the force and lateral root displacement associated with root failure, according to Meijer et al. (2017b). d_r is the root diameter, σ_t and σ_b are the root tensile and bending strength, E_t and E_b the root tensile and bending stiffness, p_u the soil resistance against root displacement and τ_i the interface friction between root and soil.

Model		Equation	Multiplication factor ξ	
			Point load	Shear load
Bending	Peak force	$F_u = \xi_1 \frac{\pi}{4} d_r^2 \sigma_b^{0.5} p_u^{0.5}$	$\xi_1 = 1.3027$	$\xi_1 = 0.5642$
	Peak displacement	$u_u = \xi_2 \frac{\pi}{4} d_r \sigma_b^2 E_b^{-1} p_u^{-1}$	$\xi_2 = 0.1249$	$\xi_2 = 1.3360$
Cable	Peak force	$F_u = \xi_3 \frac{\pi}{4} d_r^2 \sigma_t \frac{2\sqrt{\eta}}{1+\eta}$	$\xi_3 = 2$	$\xi_3 = 1$
	Peak displacement	$u_u = \xi_4 \frac{\pi}{4} d_r \sigma_t p_u^{-1} \zeta^{0.5}$	$\xi_4 = 1$	$\xi_4 = 2$

$\zeta = \frac{1}{8} \frac{\sigma_t p_u}{E_t \tau_i}$

$\eta = \sqrt{\frac{\zeta - 2\sqrt{\zeta+1}+2}{\zeta}}$

Table 2: ANOVA results for the effect of various root classes on the soil peak shear strength and normalised energy parameter in the surface layer (0–125 mm). Numbers indicate the percentage of variance explained by each root class.

		Day		Roots 0–2 mm		Roots 2–5 mm		Roots >5 mm	
		[%]		[%]		[%]		[%]	
Peak strength	Bullionfield	16.7	.	18.3	.	0.1		2.6	
	Hallyburton Hill	14.4	*	0.4		1.5		64.6	***
W_n	Bullionfield	8.5	**	30.8	***	28.9	***	18.6	**
	Hallyburton Hill	1.1		0.1		1.7		57.7	***

Figure captions

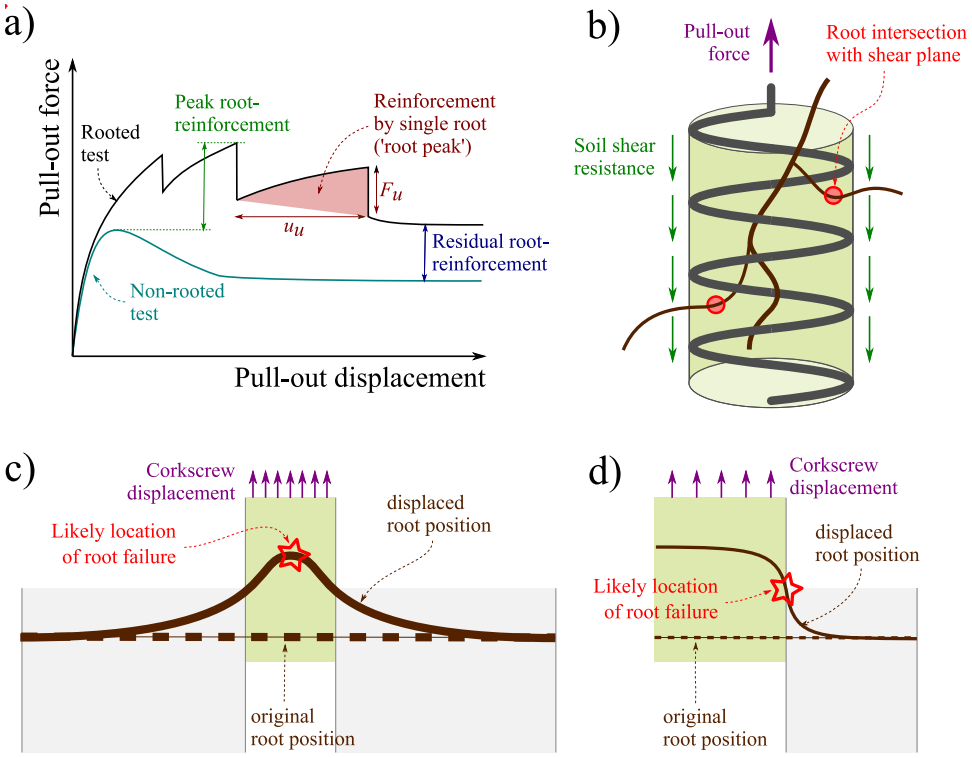

Figure 1: Schematic representation of a) corkscrew force–displacement behaviour, b) soil and root behaviour during corkscrew extraction, c) behaviour of thick roots during corkscrew extraction and d) behaviour of thin roots during corkscrew extraction.

Figure 2: Picture of the corkscrew device

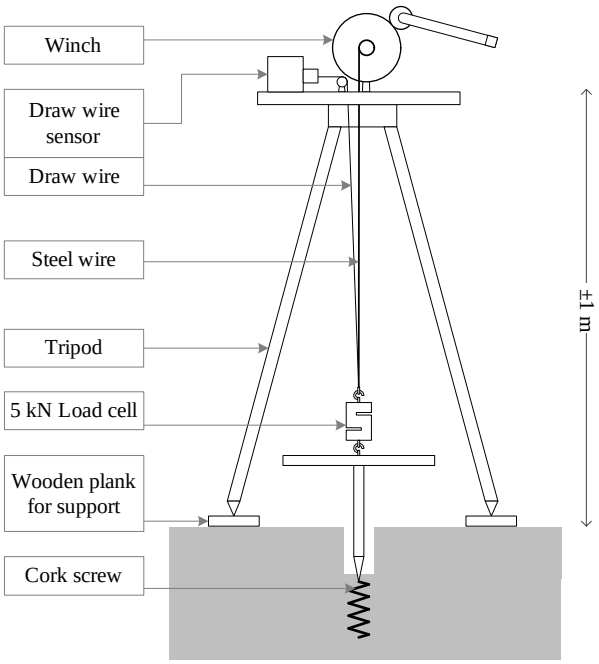

Figure 3: Schematic view of corkscrew field setup. Data was recorded using a Campbell CR3000 logger at a sampling rate of 100 Hz

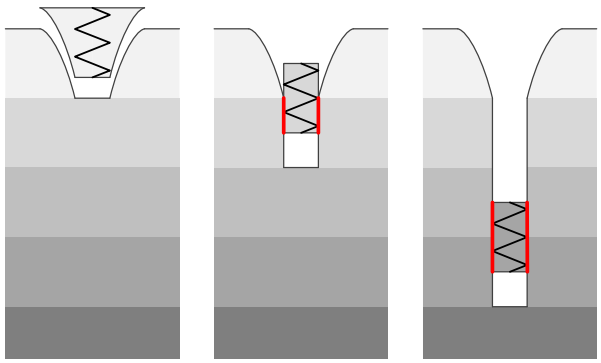

Figure 4: Development of shear area (thick red lines) during displacements at various depth levels

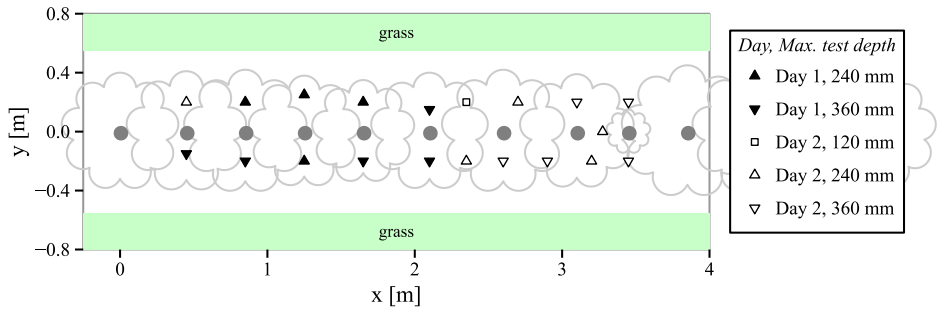

Figure 5: Locations of plots, corkscrew tests and nearby blackcurrant shrubs (solid grey circles) at Bullionfield. The shrub canopy is indicated using grey circular line segments.

Figure 6: Picture of the Bullionfield test site.

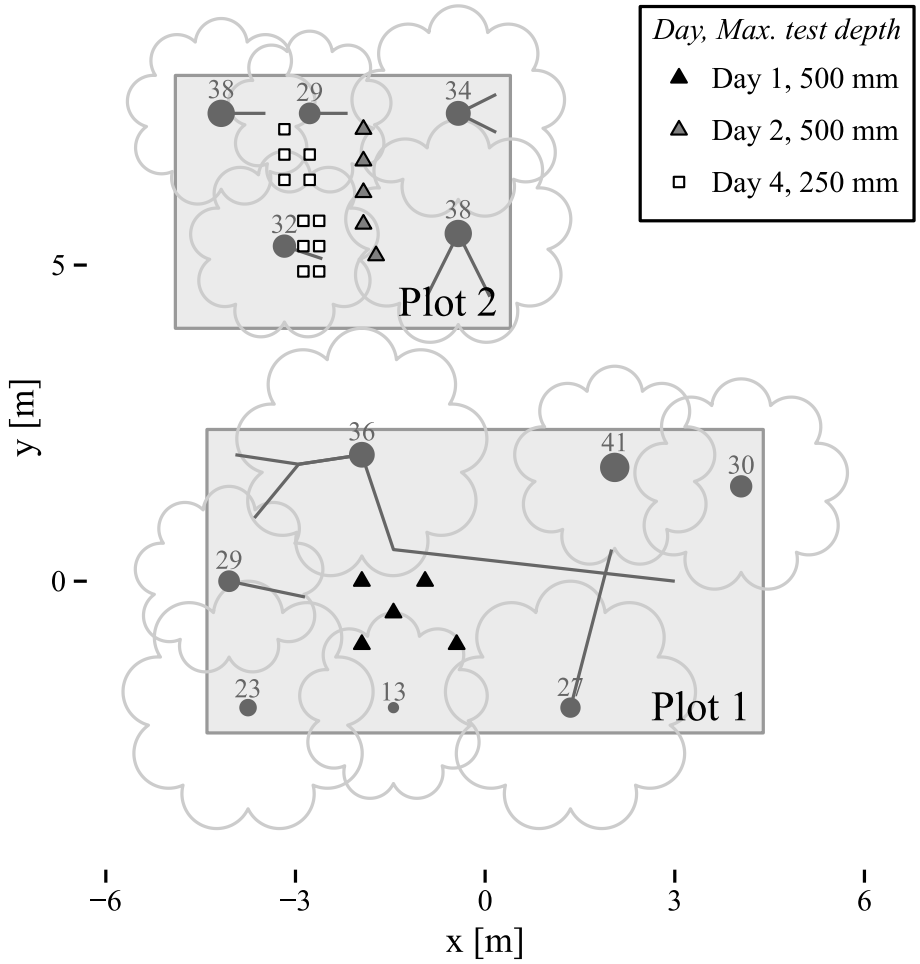

Figure 7: Locations of plots, corkscrew tests and nearby trees at Hallyburton Hill. Solid grey circles indicate nearby trees (diameter at breast height given in centimetres) and straight grey lines a rough estimate where large structural roots were exposed. The tree canopy is indicated using grey arcs. Only trees within plots are plotted.

Figure 8: Picture of the Hallyburton Hill test site.

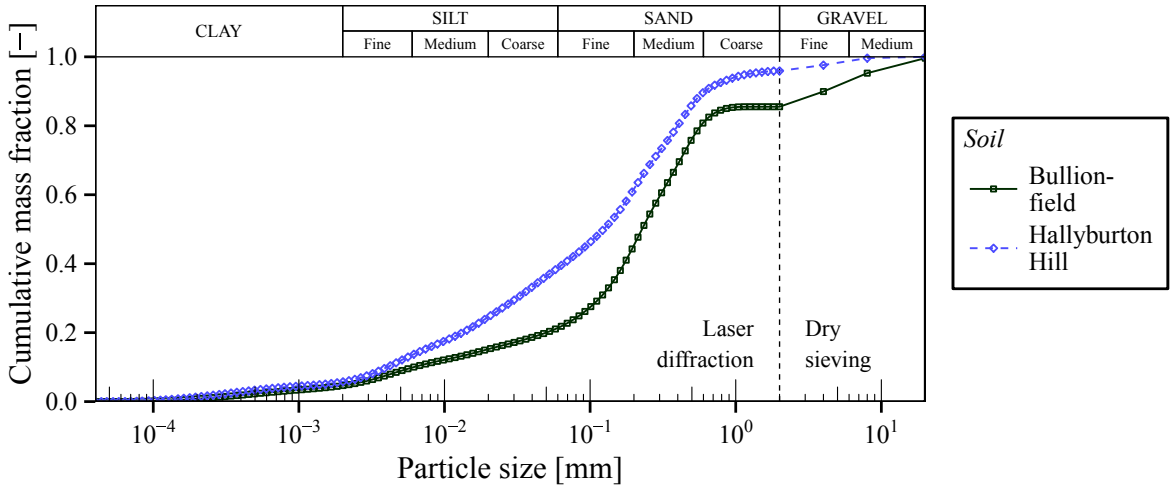

Figure 9: Particle size distributions. A laser granulometer (LS 13320, Beckman & Coulter) was used to quantify the amount of particles smaller than 2 mm, while dry sieving was adopted for particles >2 mm. Soils were sampled between 150 and 250 mm depth.

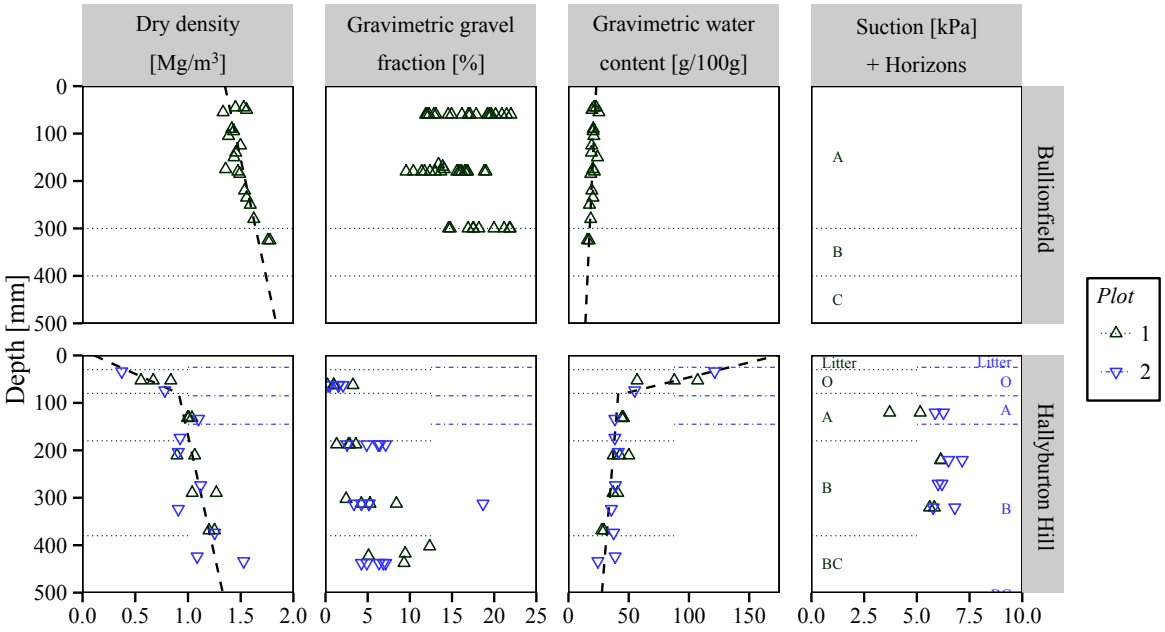

Figure 10: Water content, dry density, gravel content (>2 mm), suctions and soil horizon depths. 'O' indicates the organic soil horizon or forest floor, 'A' the topsoil layer, 'B' the subsoil layer, 'C' the layer of parent rock material and 'BC' a mixture of 'B' and 'C'.

Figure 11: Extracted foam core with trapped root ends from Hallyburton Hill

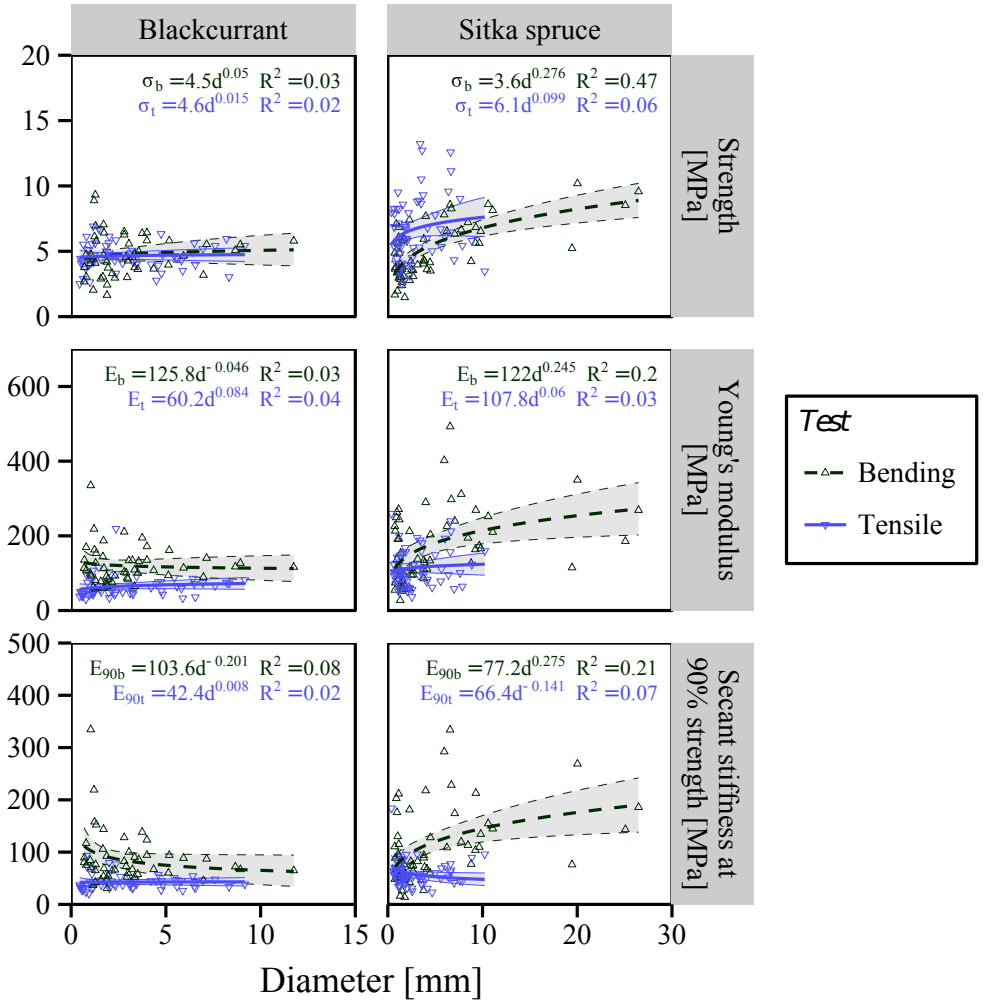

Figure 12: Root strength and stiffness in uniaxial tension and 3-point bending. Points indicate individual measurements, lines the best power law fit and shaded areas the 95% confidence interval of these fits.

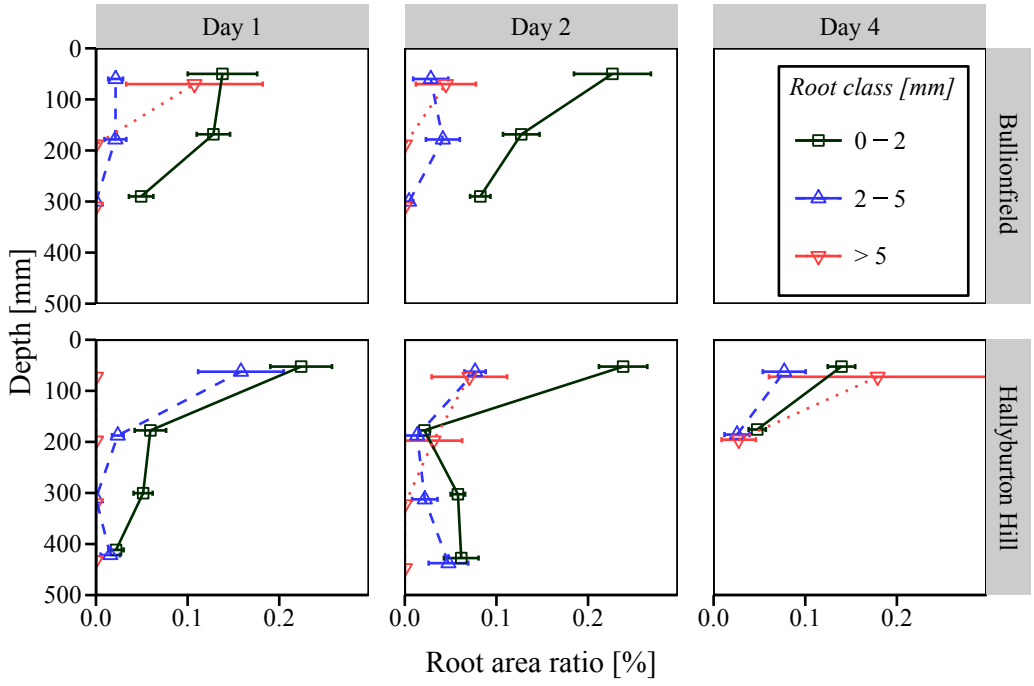

Figure 13: Average root area ratio (determined by summing counted root ends ($d_r > 2$ mm) crossing the corkscrew shear plane and WinRhizo results from the soil plug extracted using the corkscrew ($d_r \leq 2$ mm, uniform distribution assumed) for various root size classes over depth at both sites. Error bars indicate the size of one standard error.

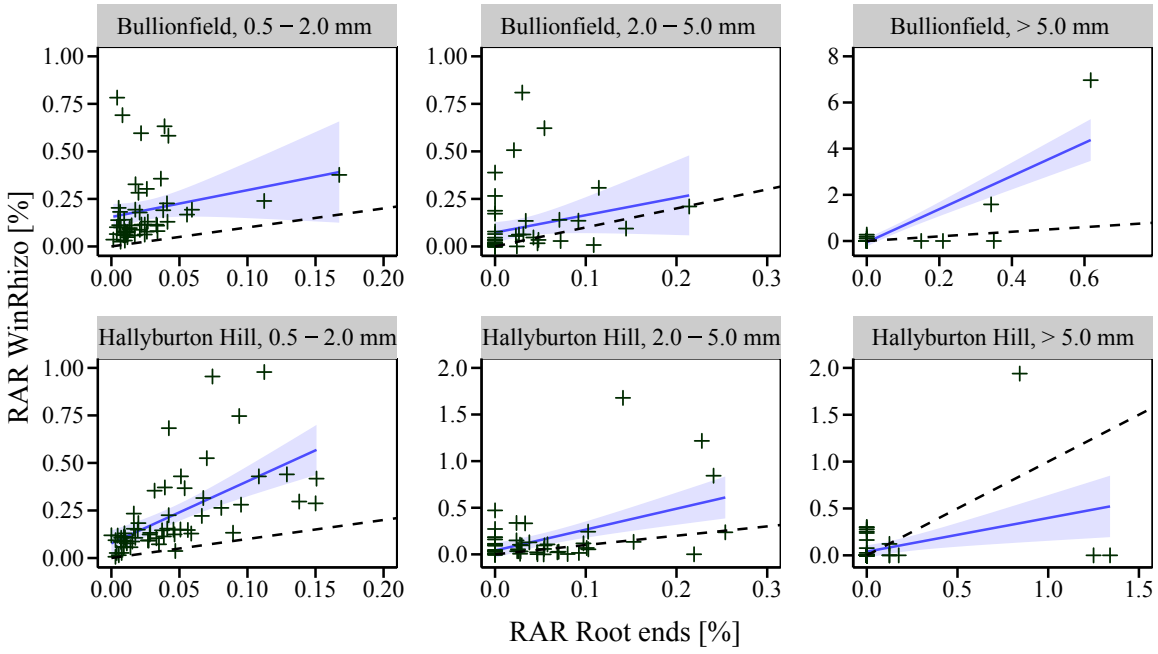

Figure 14: Comparison between root area ratios determined using WinRhizo and by counting root ends sticking out of corkscrew samples and foam cores. The dotted line indicates parity, solid lines the best linear fit and shaded areas the 95% confidence interval of this fit.

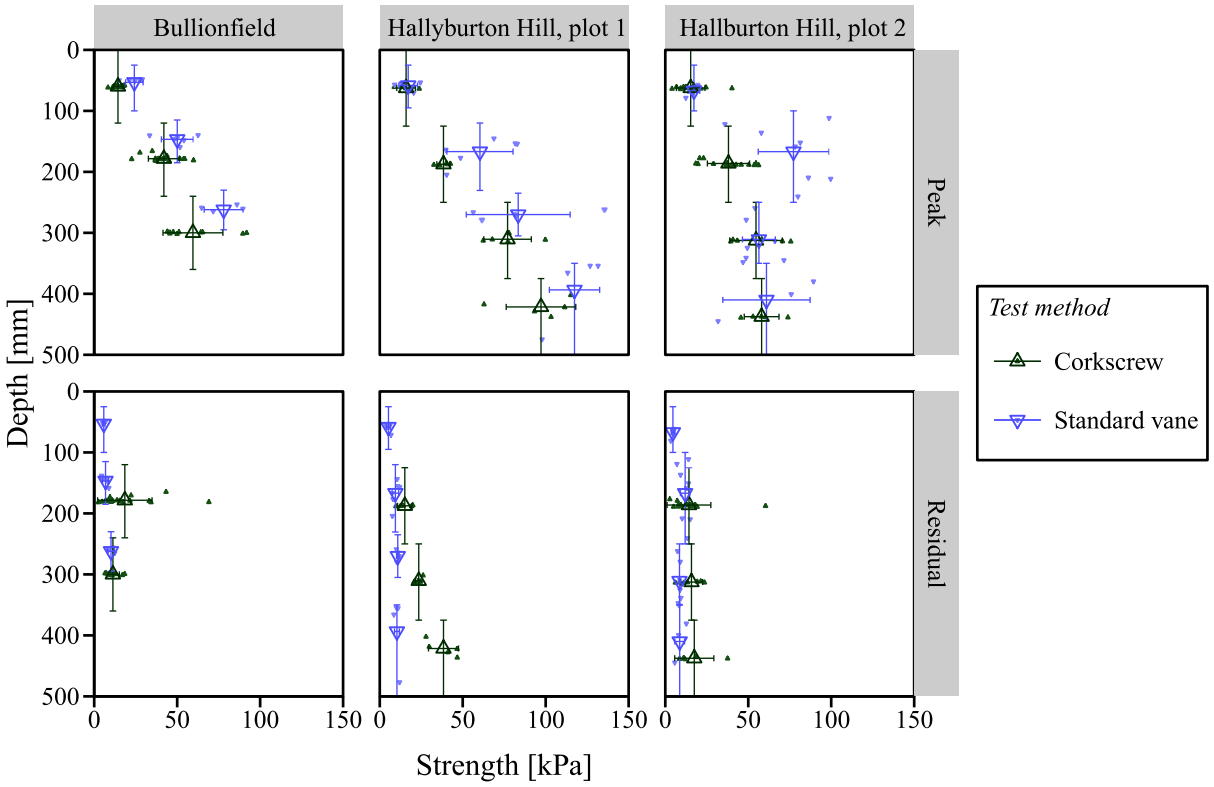

Figure 15: Comparison of corkscrew and standard vane peak shear strengths. Small symbols indicate individual measurements. Large symbols indicate averages. Horizontal error bars indicate one standard deviation, and vertical error bars the depth range over which average values are computed.

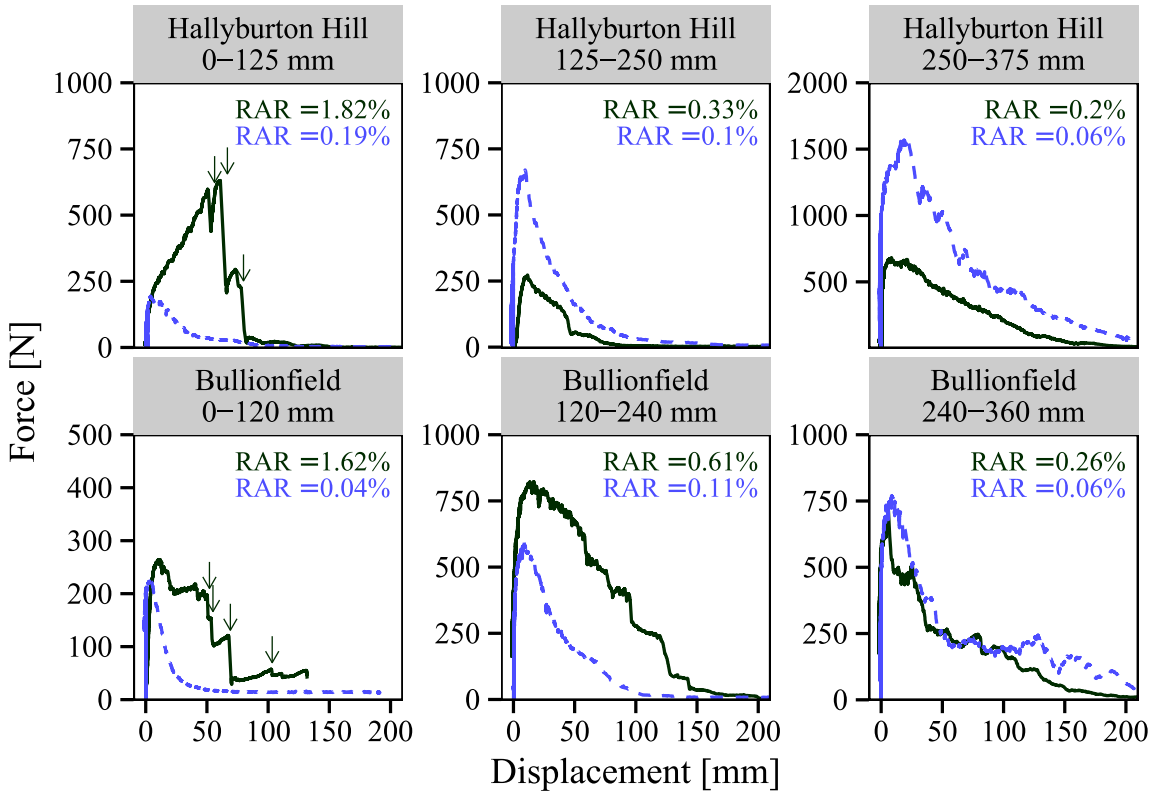

Figure 16: Example corkscrew extraction force–displacement traces. For each site and depth, the corkscrew test with the highest RAR (solid line) and the lowest RAR (dashed line) is plotted. Arrows indicate sudden drops in resistance associated with root breakages.

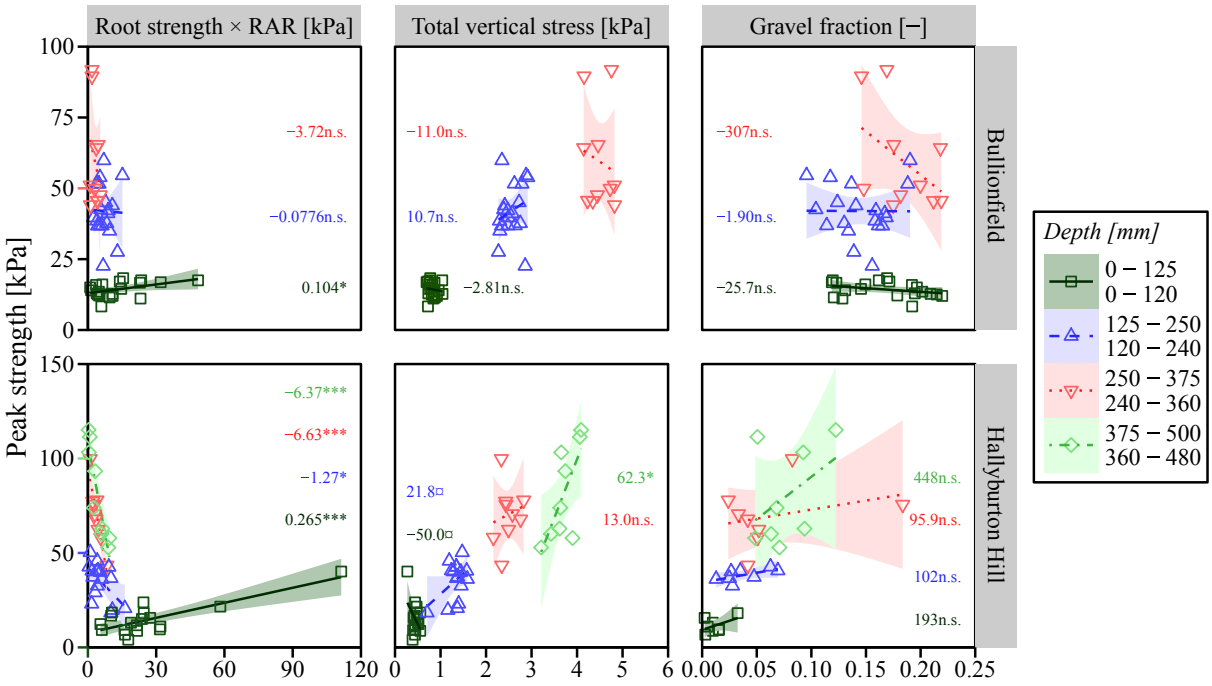

Figure 17: Corkscrew peak strength versus total root tensile strength (normalised for shear surface area), estimated vertical soil stress and gravel mass fraction for each site and depth level. Numbers denote the gradient of the linear fit. Shaded areas indicate the 95% confidence interval of the fit.

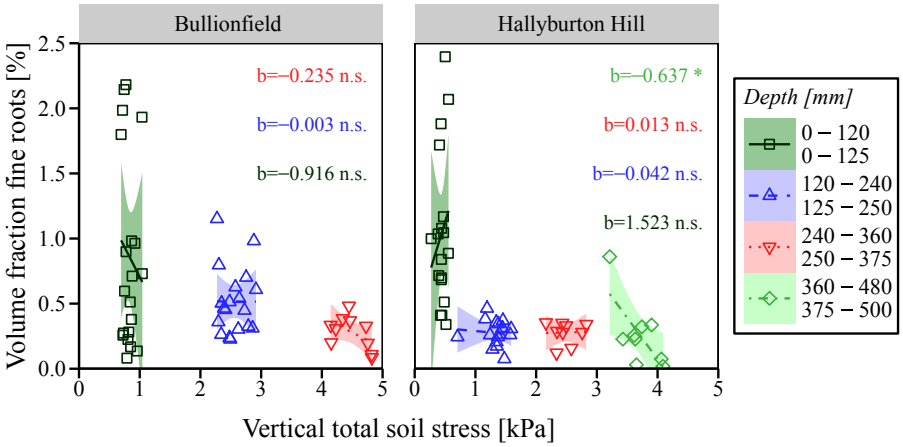

Figure 18: Root volume fraction for fine roots ($d_r \leq 2$ mm, determined using WinRhizo) as a function of total vertical soil stress. Numbers denote the gradient of the linear fit. Shaded areas indicate the 95% confidence interval of the fit.

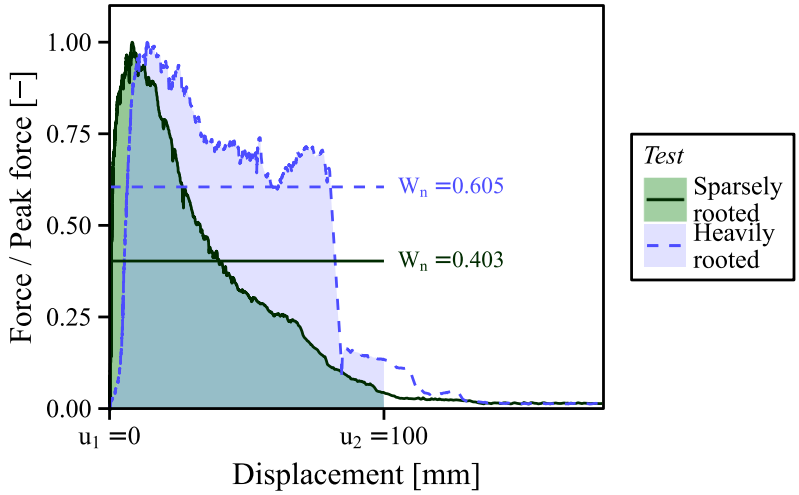

Figure 19: Visualisation of the Normalised Energy Dissipation parameter W_n for a heavily ($RAR = 0.40\%$) and sparsely rooted ($RAR = 0.11\%$) test at 120–240 mm depth at Bullionfield.

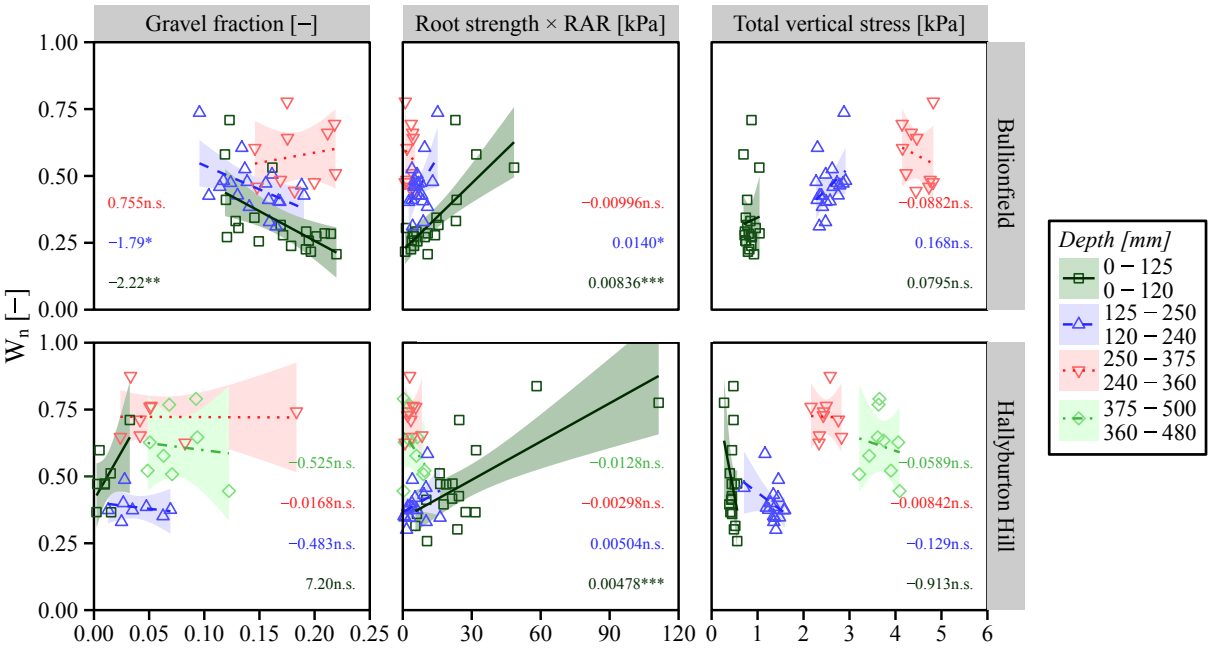

Figure 20: Normalised energy dissipation (W_n) as a function of total root tensile strength (normalised for shear surface area), estimated vertical soil stress and gravel mass fraction for each site and depth level. Numbers denote the gradient of the linear fit. Shaded areas indicate the 95% confidence interval of the fit.

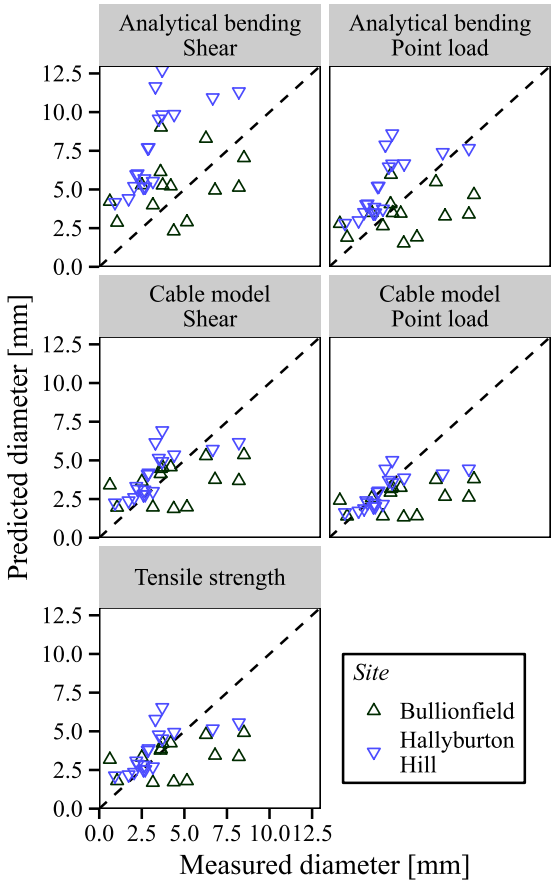

Figure 21: Comparison of diameters of individual roots measured and predicted based on the magnitude of the sudden decrease in corkscrew resistance ('force drop' F_u). The dashed lines indicate parity, coloured lines linear fits and shading the 95% confidence interval of these fits

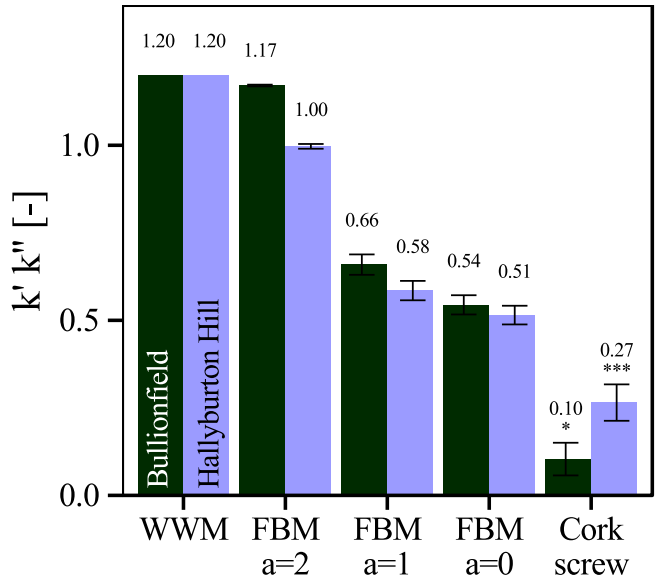

Figure 22: Comparison of model and experimental root-reinforcement results. Root-reinforcement is normalised over the product of root tensile strength σ_t and root area ratio RAR (this is equal to the product of k' and k'', see Equation 5). a refers to the FBM load distribution parameter, see Equation 4. For experimental results, the gradient, standard error and statistical significance of the linear fit between $\sum \sigma_t RAR$ and τ_{cs} is given. For model results, the mean and standard error (error bars) of predicted values for $k'k''$ is given, assuming $k' = 1.2$

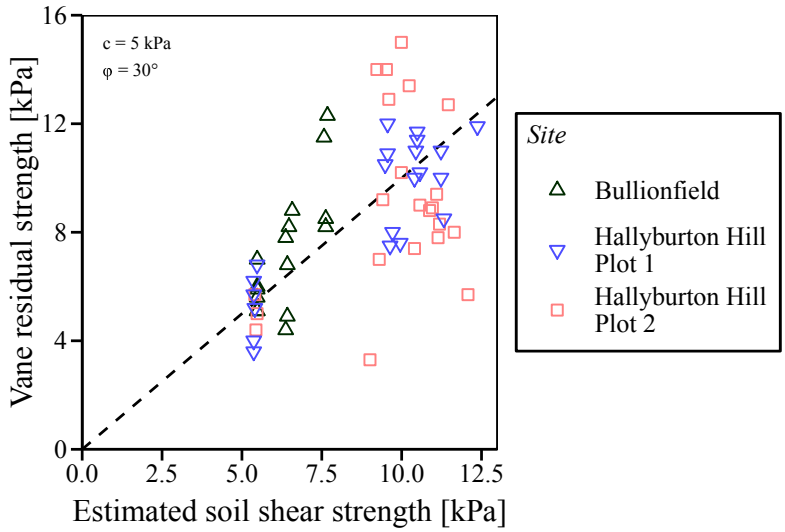

Figure 23: Comparison between measured vane residual strength and model values. The dashed line indicates parity. Suction levels were taken as $s = 0$ kPa in Bullionfield. In Hallyburton Hill, $s = 0$ kPa and 6 kPa below 80 mm depth.

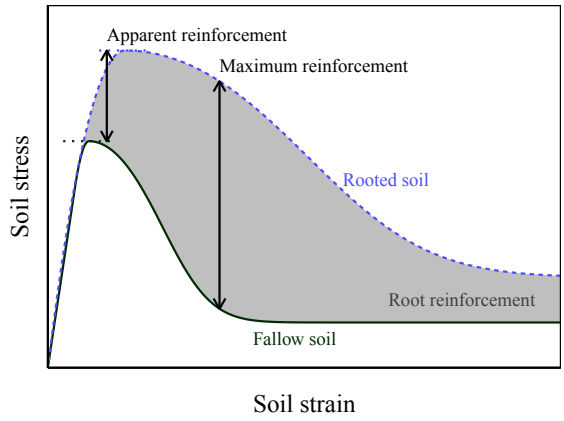

Figure 24: Schematic rooted and non-rooted soil stress–strain curves.

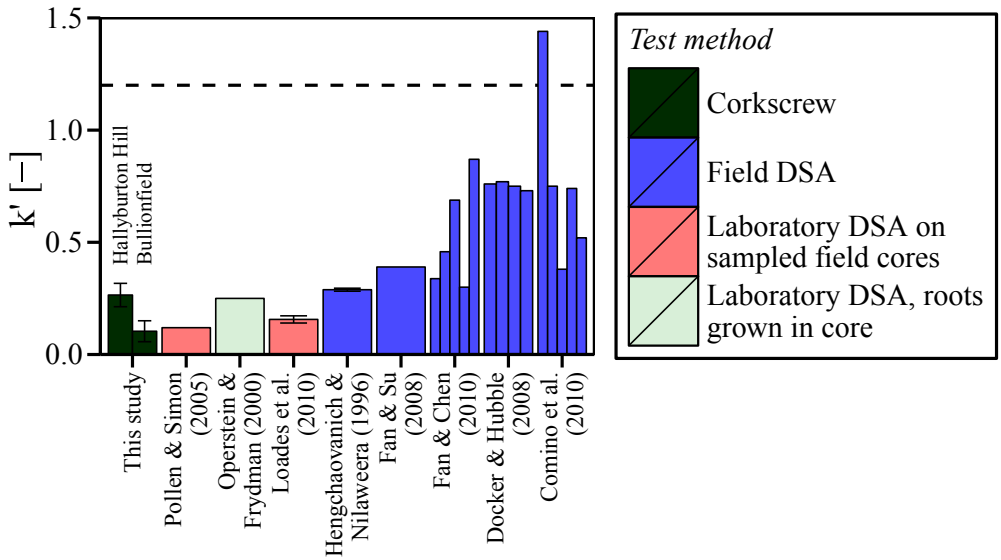

Figure 25: Comparison of values for k' (from Equation 2) found in the surface layers (0–120/125 mm) at Bullionfield and Hallyburton Hill against direct shear testing ('DSA') reported in the literature. k' is defined as $c_r / \sum \sigma_t RAR$, see Equation 2. The dotted line indicated the WWM solution where $k' = 1.2$. Field core data from Loades et al. (2010) was re-analysed to find k'. Values for k' for Hengchaovanich and Nilaweera (1996) were found by re-analysing their reported data and the value for Pollen and Simon (2005) by analysing the gradients in their plotted data.